Supplemantary Information

Modulated thermal conductivity of 2D hexagonal boron arsenide: emerged strain-induced study

Mostafa Raeisi [a], Somaieh Ahmadi [*c], and Ali Rajabpour [*a,b]

a. Department of Mechanical Engineering, Imam Khomeini International University, Qazvin, Iran.

b. School of Nano Science, Institute for Research in Fundamental Sciences (IPM), P.O. Box 19395-5531, Tehran, Iran

c. Department of Physics, Imam Khomeini International University, Qazvin, Iran.

Email: Rajabpour@eng.ikiu.ac.ir

Section.S1: Uniaxial strain modeling

In this work, uniaxial tensile strain is applied to the structure. The uniaxial strain is implemented by increasing the lattice vector (lattice constant, LC, in the straining directions). Then, the other perpendicular direction is relaxed. In other word, by fixing the lattice constant along the strain direction, the simulation cell in the other direction is relaxed to zero stress and zero forces for all embedded atoms. For instance, by stretching the structure alongside the armchair direction, i.e. increasing the lattice constant in the armchair direction and then fixing it, the other direction, i.e. the lattice constant of the zigzag direction (LC^{zig}), is free to resize. In addition to the LC^{zig}, the atomic positions are also free to move and optimized till minimum energy threshold achieved. Figure.S1 shows the unstrained and 7%-Arm (strain alongside the armchair direction). Regard to this figure, for unstrained structure: a=b= 1.955 Å, c=120°, for the strained 7%-Armchair: a= 2.064 Å, b= 1.983 Å, c= 114.5°, and for the strained 7%-Zigzag: a= 1.957 Å, b= 2.034 Å, c= 125.9°. The lattice constants alongside the armchair direction calculated as 2.932 Å, 3.137 Å, 2.882 Å whereas alongside the zigzag direction calculated as 1.693 Å, 1.668 Å, 1.811 Å for unstrained, 7%-Arm strained, and 7%-Zig strained, respectively.

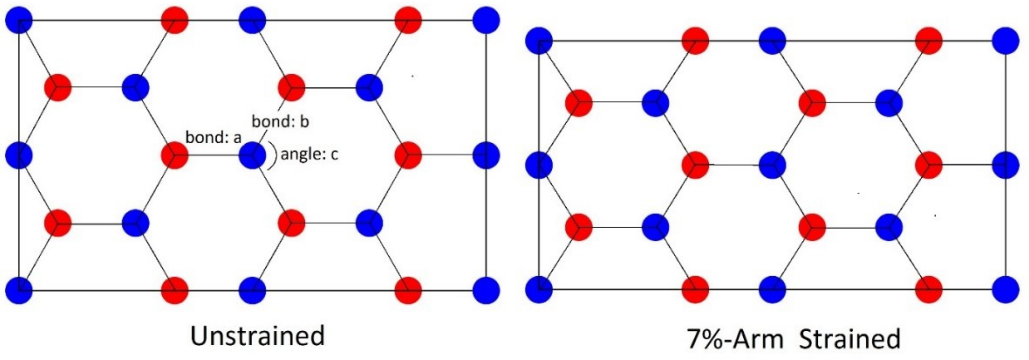

Figure S1: Uniaxial strain modeling of h-BAs. For instance, in the strained structure alongside the armchair direction, the armchair's lattice constant increased and then fixed while the prependicualr direction, i.e. the zigzag, is free to resize. The atomic positions are free to move till minimization threshold occurrs.

Section.S2: Mechanical Properties

To evaluate the mechanical properties, i.e. the elastic modolus and Poisson's ratio, we used the uniaxial tensile strain model as we explain in Section.S1. Figure.S2 shows the varying energy versus the uniaxial tensile strain. The complementary explanation could be found in section 3.2 of the main paper.

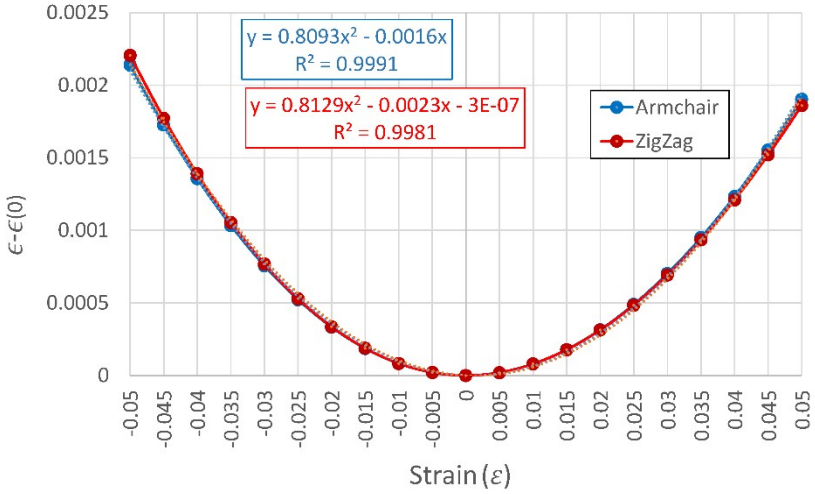

Figure S2: Volume specific energy versus uniaxial tensile strain in both zigzag and armchair directions

Section.S3: Band Structure

By increasing the uniaxial tensile strain in both armchair and zigzag directions, the band gap will increase as 0.97, 0.985, 1.02, and 1.03 (eV) with respect to the unstrained, 3%-, 5%-, and 7%-strained structures. The tensile strain in different directions has no impact on the band gap, and it is negligibly subjected to the percentage of uniaxial tensile strain.

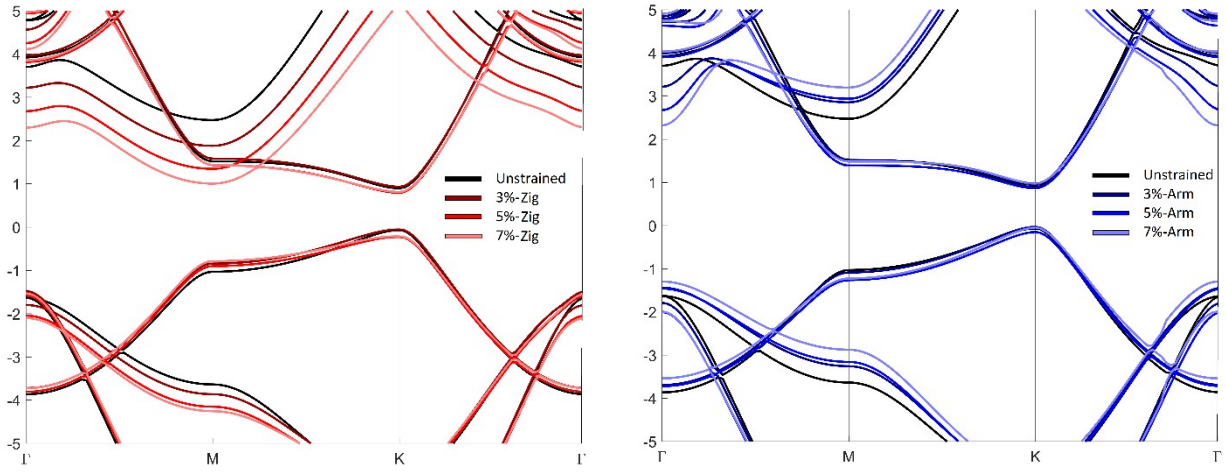

Figure S3: Electronic band structure under uniaxial tensile strain up to 7% along the zigzag (Left, red) and the armchair (Right, blue) directions.

Section.S4: Phonon Dispersion and Partial Density of States

The phonon dispersion relation is depicted in Figure.S4 and the partial density of states is also shown in Figure.S5. By increasing the strain, the maximum optical energy and the a-o gap value decrease and LA and TA branches shift to the lower group velocity. The black line is for the unstrained sample, and lighter blue (or red) is for the maximum strained sample, i.e. 7%-Arm (or 7%-Zig).

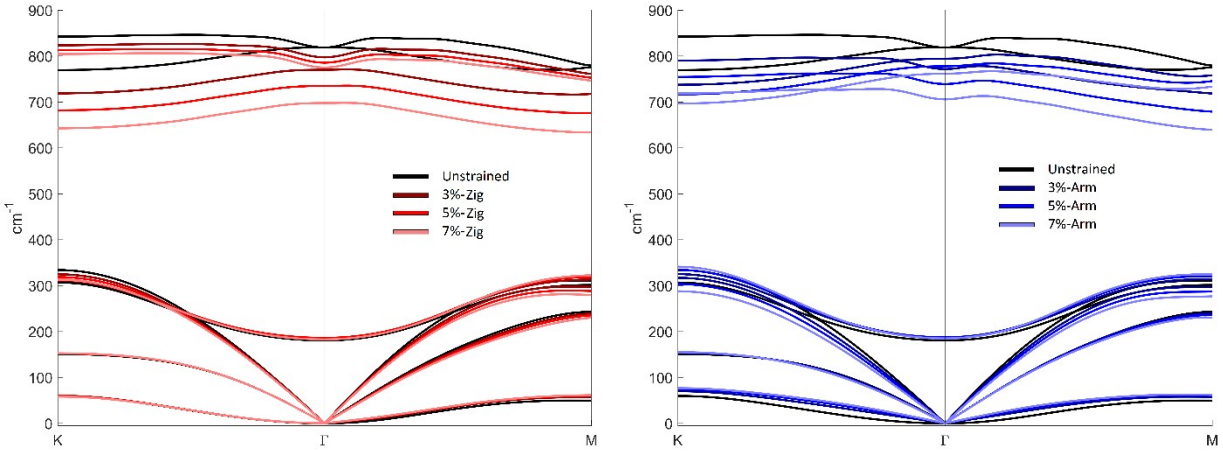

Figure S4: Phonon dispersion under uniaxial tensile strain up to 7% along the zigzag (Left figure) and the armchair (Right figure) directions.

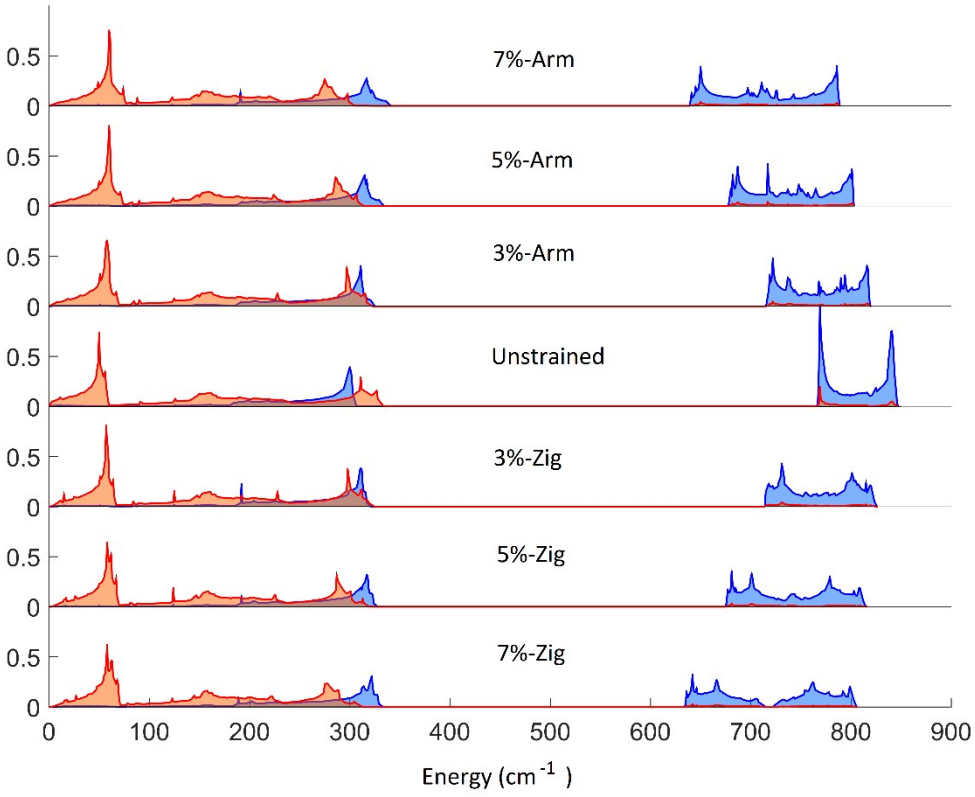

Figure S5: Phonon partial density of states under uniaxial tensile strain up to 7%. The middle curve is for the unstrained sample. Toward the top and bottom, the strain is increased along the armchair and zigzag, respectively.

Table S1: Summarized energy of a-o gap, maximum of four lower bands, and minimum of two upper bands as shown in the phonon dispersion figure

	Frequency (cm^{-1})						
	7%-Zig	5%-Zig	3%-Zig	unstrained	3%-Arm	5%-Arm	7%-Arm
Max. energy of four lower bands	322.5	318.7	324.6	333.9	325.0	334.3	341.1
a-o gap	311.3	357	391.6	435.5	393.4	344.6	298.4
Min. energy of two upper bands	633.8	675.7	716.2	769.4	718.4	678.9	639.5

Section.S5: Q-size and neighboring impact (studying the thermal conductivity convergence)

The q-grid study is depicted in Figure.S6. The unstrained structure of h-BAs is completely converged in the grid size of 50x50x1 (Figure.S6 a). Applying strain alongside the armchair and zigzag directions have different behaviors. In the zigzag direction, the thermal conductivity is tending to converge, while in the armchair one, the divergence is pretty observable for higher strain values. In the previous investigation of the uniaxial strained graphene, Pereira and Donadio observed that uniaxial stretching alongside the armchair direction is diverged by increasing the q-size, at room temperature [1]. They concluded that uniaxial tensile strain reduces ZA phonon population, make the group velocity finite, and increases phonon lifetime at low frequencies nearby gamma point (zone center). In the present study, we observe this divergent trend alongside the armchair direction for the strain values greater than 3% (Figure.S6 b). The q-grid study shows the intensive sensitive behavior of the thermal conductivity as a function of q-grid size in the uniaxial armchair direction. In contrary, the uniaxial tensile strain alongside the zigzag direction shows stable and consistency behavior regards to varying q-size of phonon wave-vectors with the inclination to the convergence (for thermal conductivities in both zigzag and armchair directions as shown in Figure.S6 d and Figure.S6 e). The thermal conductivities alongside the zigzag direction in the uniaxial armchair strained structures are converged too (Figure.S6 c).

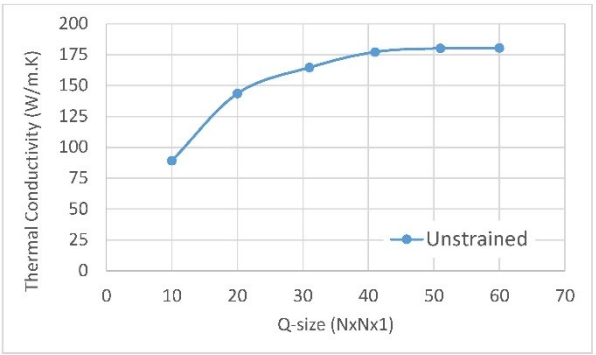

(a)

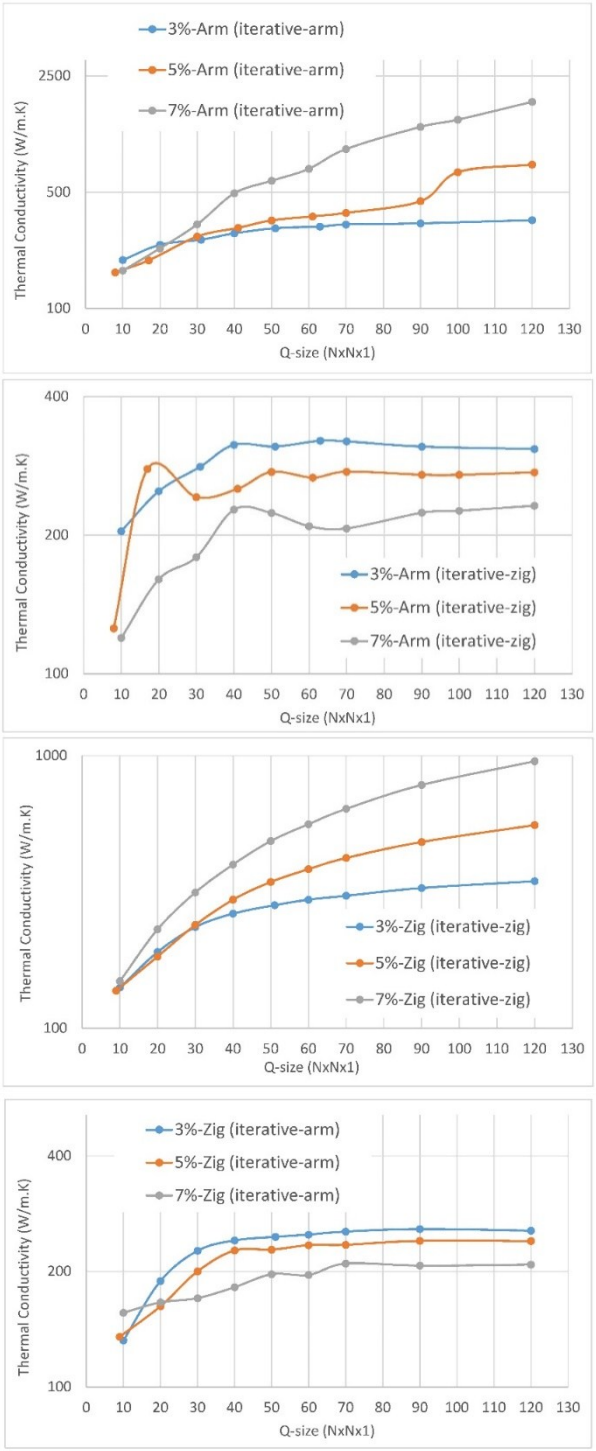

Figure S6: Q-size dependency of the thermal conductivity for all simulations,
a) unstrained structures,
b) uniaxial tensile strain along the armchair direction (thermal conductivity reported for the armchair direction),
c) uniaxial tensile strain along the armchair direction (thermal conductivity reported for the zigzag direction),
d) uniaxial tensile strain along the zigzag direction (thermal conductivity reported for the zigzag direction),
e) uniaxial tensile strain along the zigzag direction (thermal conductivity reported for the armchair direction)

In Figure.S7, four simulation test cases which incline to converge are illustrated. To acquire the converged thermal conductivity at infinite q-size, the inverse rule is used for each sample. The converged thermal conductivities are 374.95, 406.17, 979.43, and 3194.89 (W/m.K) for 3%-Arm (arm), 3%-Zig (zig), 5%-Zig (zig), and 7%-Zig (Zig), respectively.

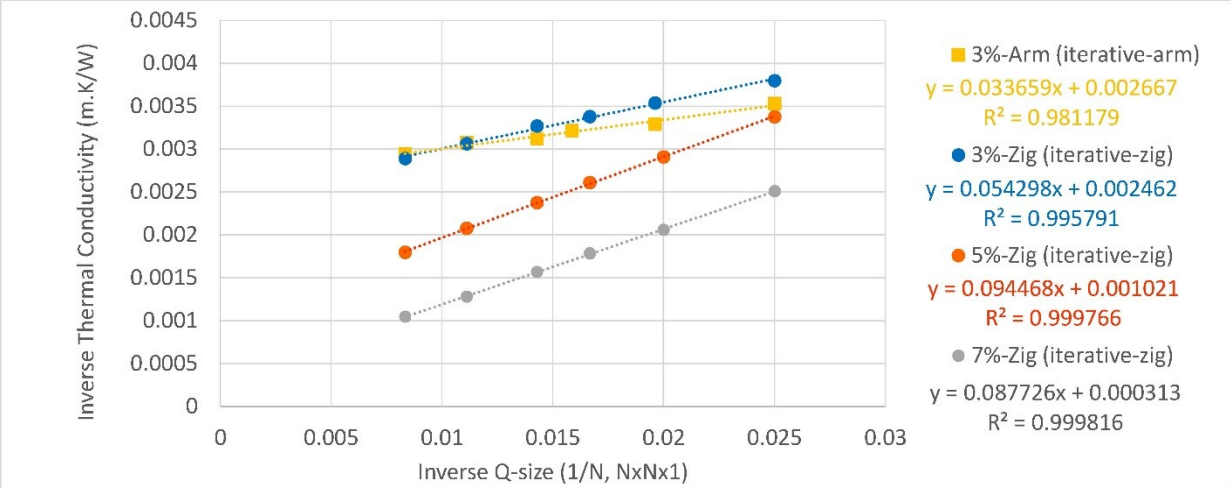

Figure S7: Inverse thermal conductivity versus inverse q-size to obtain the converged thermal conductivity

The impact of neighboring on the convergence is depicted in Figure.S8. In this study, we hired a supercell of 5x5x1. As shown in Figure.S8, the 4th neighbors suddenly increase the thermal conductivity which can not be trusted. The impact of the neighboring is calculated up to 11th neighbor's atom and illustrated the converging in the thermal conductivity (after 4th and 5th). In conclusion, 3rd neighboring shell proved to be practical (not expensive) and reliable for this problem.

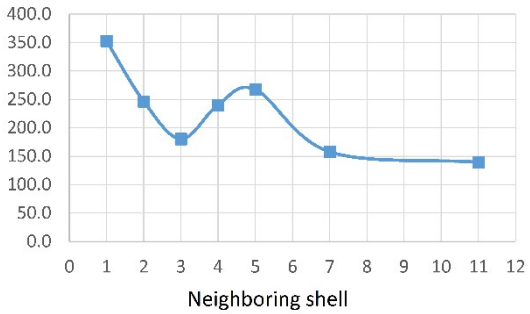

Figure S8: Impact of neighboring atoms on the convergence of the thermal conductivity for the unstrained sample

Section.S6: Cumulative Thermal Conductivity

The cumulative thermal conductivity is shown in Figure.S9. Obviously, by considering Figure.S6 (b and d), it is shown that 7%-strained structures are not converged at the mean free path of 1mm-10mm. In this picture, we can see that the thermal conductivity in the perpendicular direction to the uniaxial strain direction is converged at low MFP.

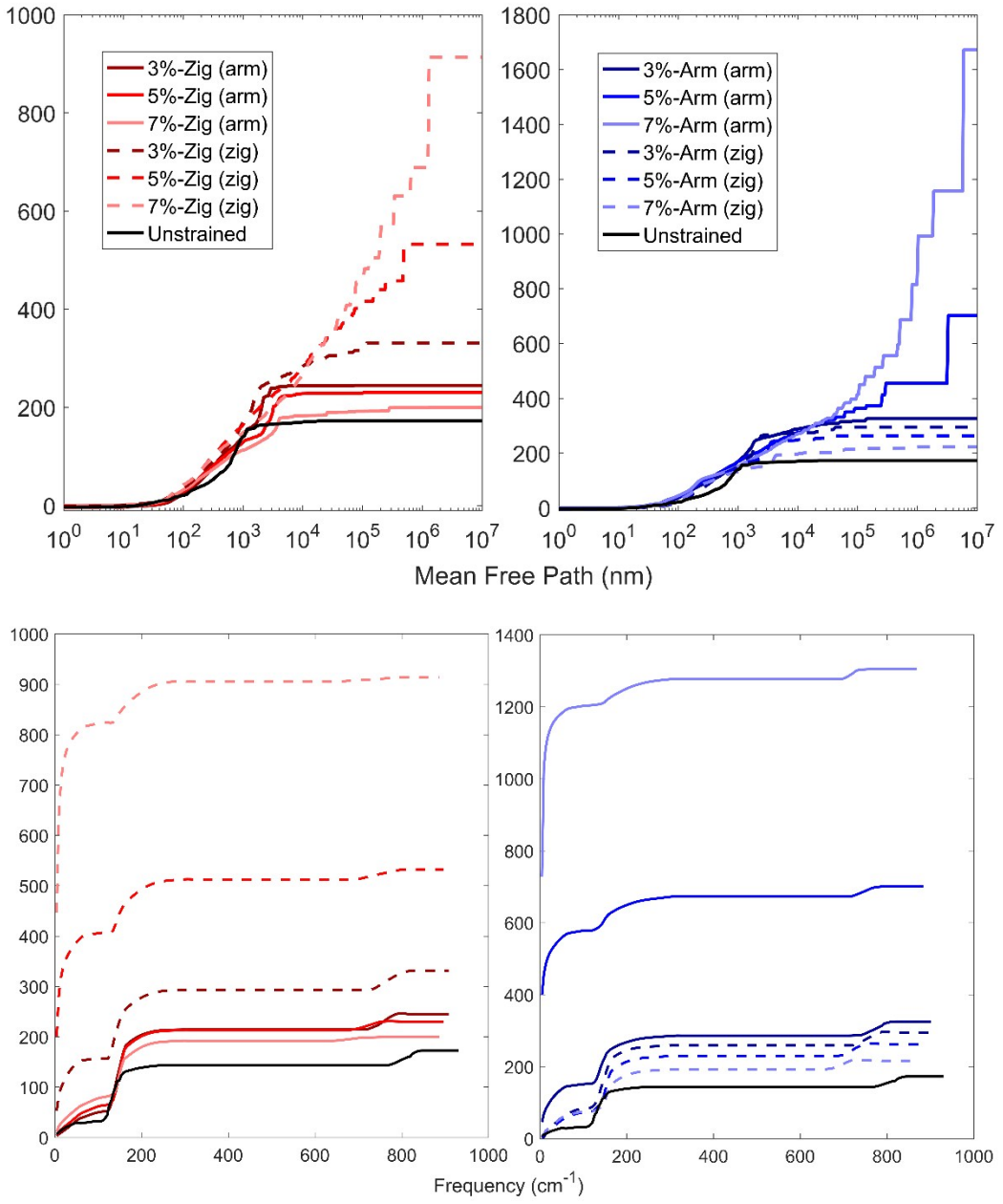

Figure S9: Cumulative thermal conductivity with respect to the mean free path (top) and the phonon frequency (bottom)

Section.S7: Contribution of each phonon mode in the Thermal Conductivity

The modal contribution of the thermal conductivity for the uniaxial tensile strain in both zigzag and armchair directions is illustrated in Figure.S10 at the room temperature. Here, Data is adopted from q-size of 120x120x1 for the strained structures and 50x50x1 for the unstrained one. As seen, by increasing the strain, ZA contribution increases drastically.

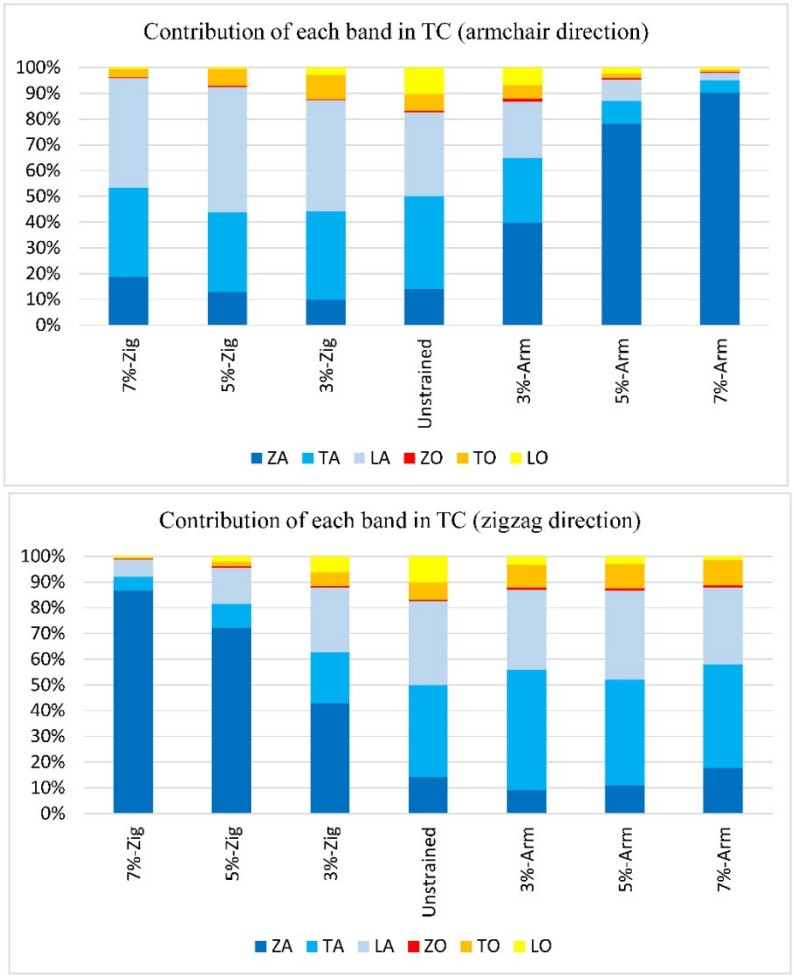

Figure S10: Modal contribution to the thermal conductivity for unstrained and strained (3%-5%-7%) structures at 300 K. The thermal conductivity presented alongside the armchair direction (top) and zigzag direction (bottom)

Table S2: Summarized thermal conductivity contribution (%) of ZA branch in the strained structures

	7%-Zig	5%-Zig	3%-Zig	unstrained	3%-Arm	5%-Arm	7%-Arm
Along the armchair direction	18.8	13	10	14.1	39.6	78.3	90.2
Along the zigzag direction	86.8	72.2	43	14.1	9	10.8	17.7

Section.S8: Phonon characteristic analysis in the reciprocal lattice

As depicted in Figure.9, four phonon characteristics, i.e. the Grüneisen parameter, phonon lifetime, group velocity, and weighted phase space are shown here for all six strained and unstrained structures in Figure.S11, Figure.S12, and Figure.S13 at the room temperature. Since the optical mode contribution in the thermal conductivity is negligible, only acoustic branches are discussed here. The flexural ZA branch is located in Figure.S11, and two other in-plane acoustic branches (LA and TA) are demonstrated in Figure.S12 and Figure.S13, respectively. The color bar for all contours is shown in Figure.S11. It should be noted that all values are normalized between their minimum and maximum to make them comparable. The normalization is done separately for each parameter in each mode. Before the normalization, due to the diverse wide order of magnitude, the natural logarithm function is used to make them linear as the color bar ranges from zero to one. For the unstrained structure, we use the q-size of 50x50x1 while for the others, 120x120x1 is adopted.

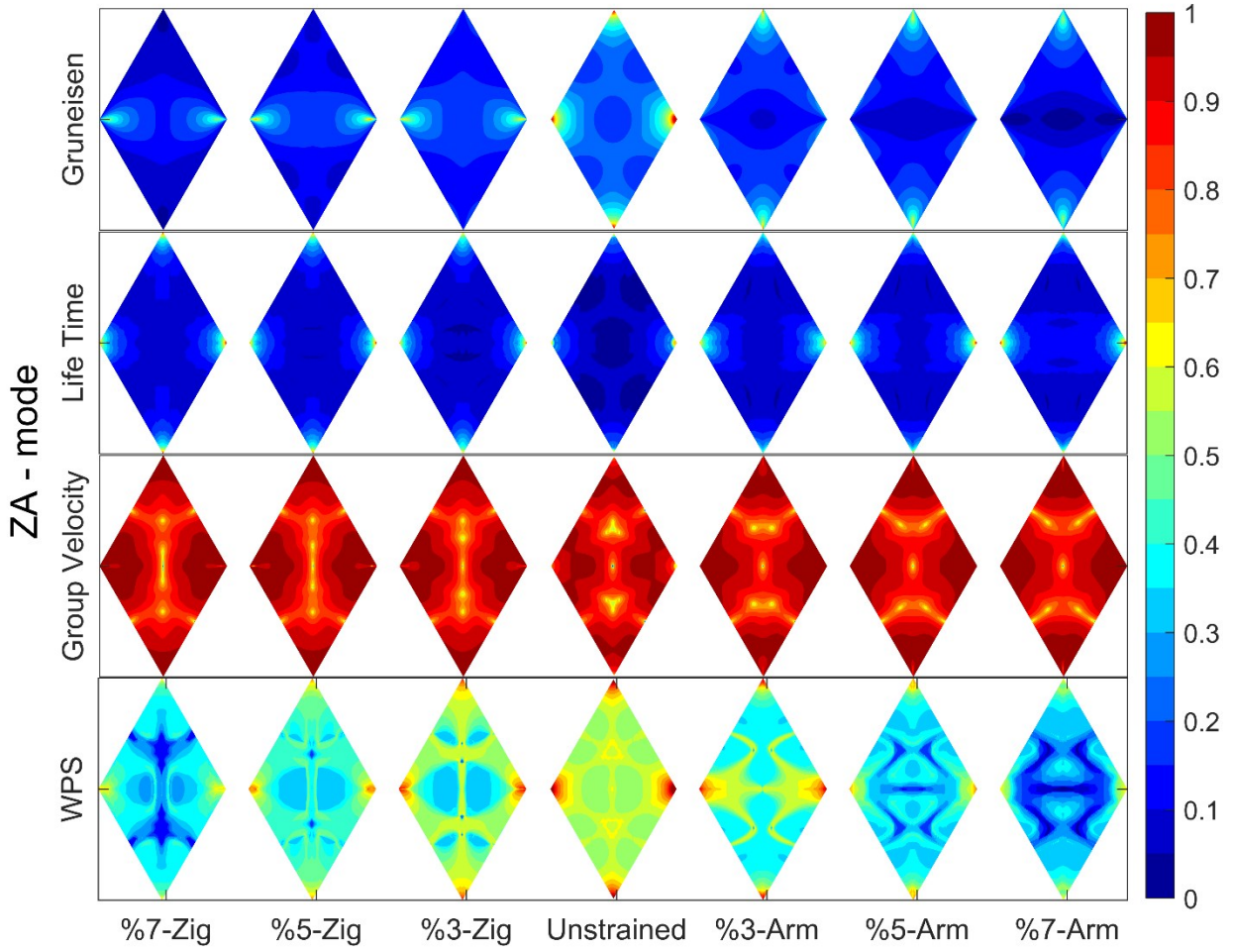

Figure S11: Grüneisen parameter, phonon lifetime, group velocity, and weighted phase space for the unstrained and different uniaxial tensile strains in both armchair and zigzag directions up to 7% strain at 300 K for the ZA mode.

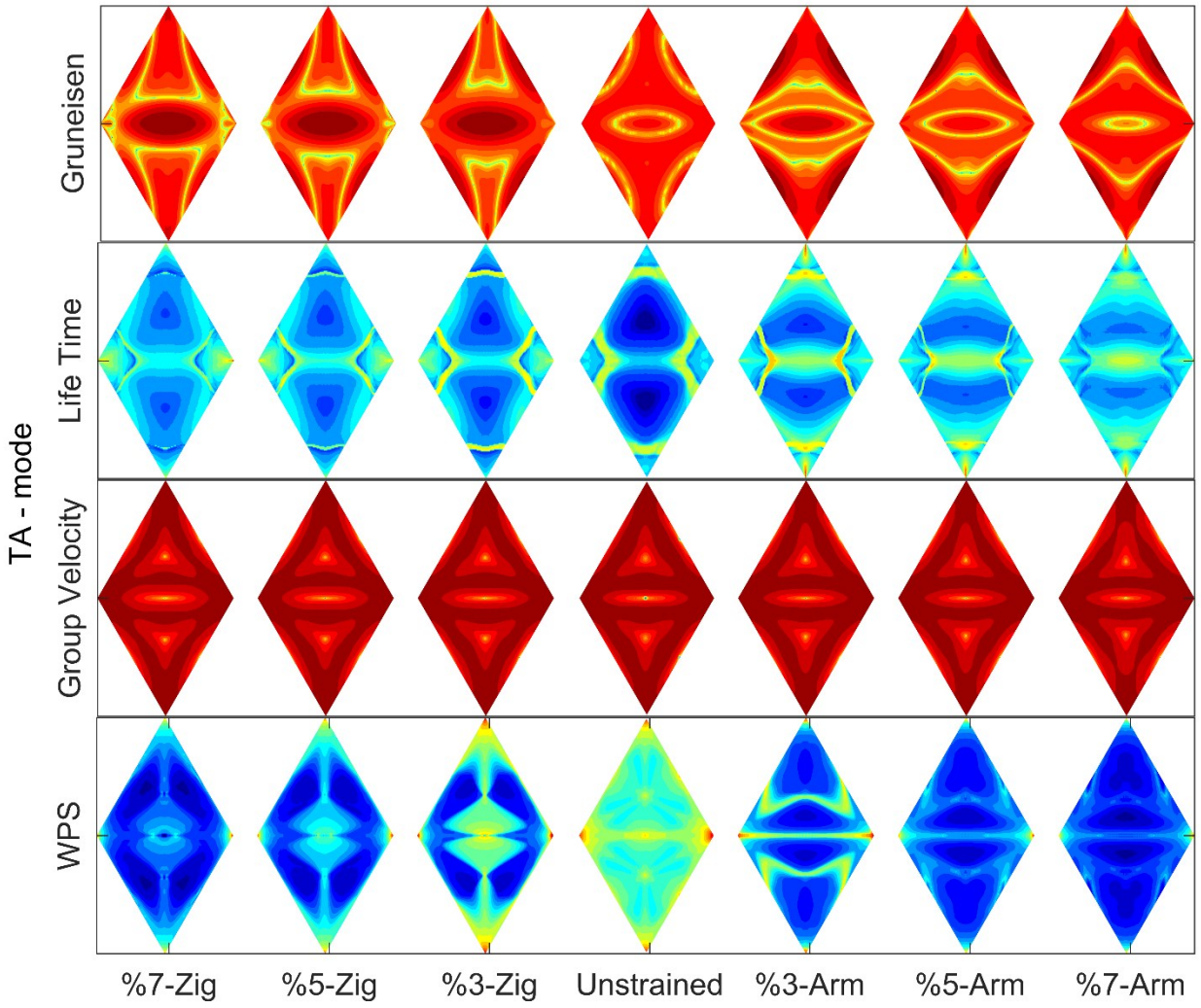

Figure S12: Grüneisen parameter, phonon lifetime, group velocity, and weighted phase space for the unstrained and different uniaxial tensile strains in both armchair and zigzag directions up to 7% strain at 300 K for the TA mode.

It should be remembered that 5%-Arm and 7%-Arm test cases showed the unstable behaviors when the q-size increases. At the maximum hired 120x120x1 q-size, the 5%-Zig and 7%-Zig test cases did not converge. But generally, for all the triple figures of Figure.S3, the trend of contours could be contenting, from unstrained structures toward 7%-strained structures in each direction.

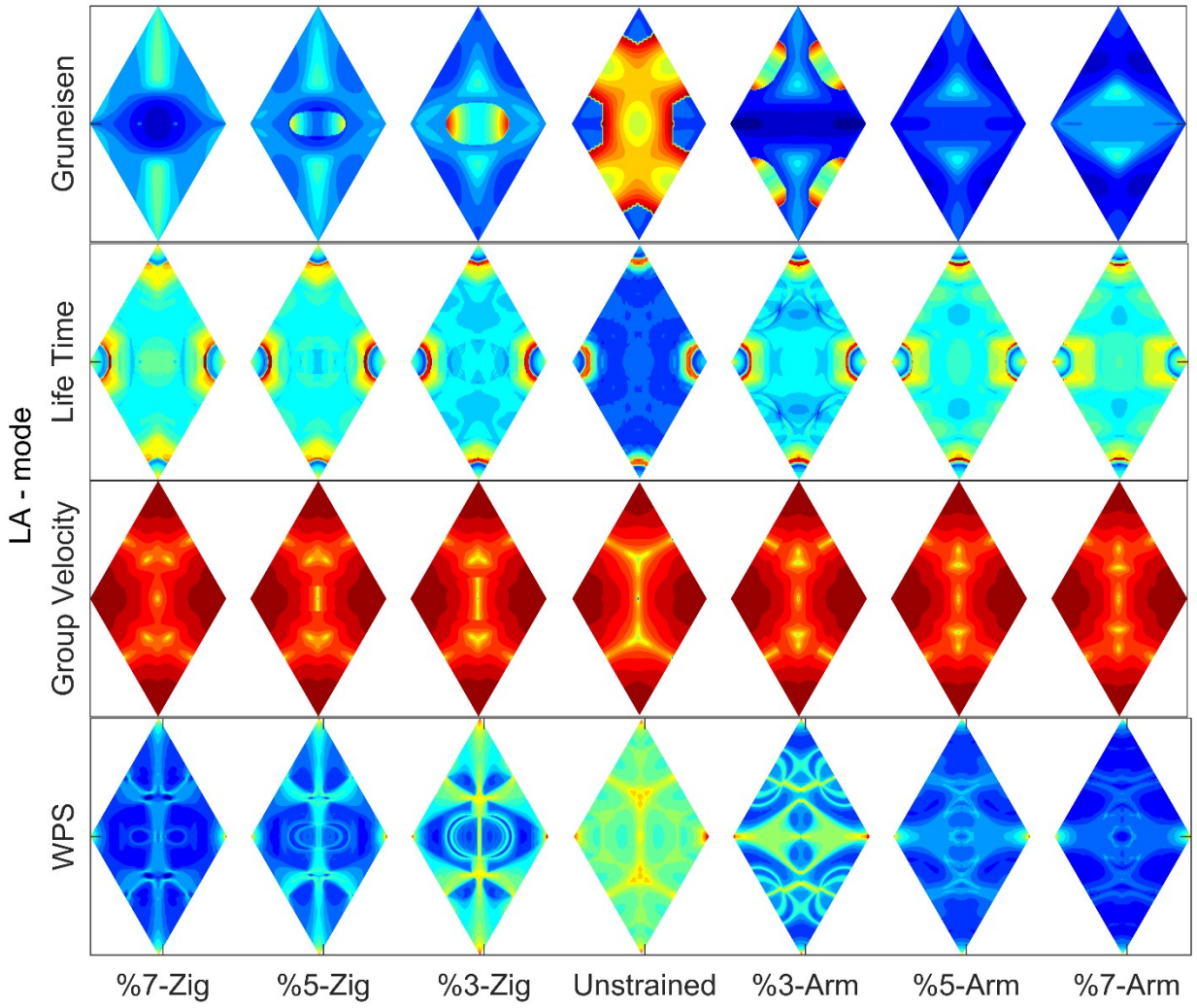

Figure S13: Grüneisen parameter, phonon lifetime, group velocity, and weighted phase space for the unstrained and different uniaxial tensile strains in both armchair and zigzag directions up to 7% strain at 300 K for the LA mode.

In Figure.S11, Figure.S12, and Figure.S13, the reciprocal lattice, the armchair direction is alongside the two opposite horizontal corners of Trapezius, and perpendicularly, the zigzag direction is alongside the two opposite vertical corners.

References

[1] L.F.C. Pereira, D. Donadio, Divergence of the thermal conductivity in uniaxially strained graphene, Phys. Rev. B - Condens. Matter Mater. Phys. 87 (2013). doi:10.1103/PhysRevB.87.125424.

-